Research Article | Vol. 27, No. 21 | 14 Oct 2019 | OPTICS EXPRESS 30371
Optics EXPRESS

High-quality single crystal diamond diffraction gratings fabricated by crystallographic etching

MARCELL KISS,[1,*] TEODORO GRAZIOSI,[1] ADRIEN TOROS,[1] TORALF SCHARF,[2] CHRISTIAN SANTSCHI,[2] OLIVIER J. F. MARTIN,[2] AND NIELS QUACK[1]

[1]EPFL, STI IMT GR-QUA, Lausanne 1015, Switzerland
[2]EPFL, STI IMT NAM, Lausanne 1015, Switzerland
*marcell.kiss@epfl.ch

Abstract: We demonstrate a novel method for fabricating single crystal diamond diffraction gratings based on crystallographic etching that yields high-quality diffraction gratings from commercially available <100> diamond plates. Both V-groove and rectangular gratings were fabricated and characterised using scanning electron microscopy and atomic force microscopy, revealing angles of 57° and 87° depending on the crystal orientation, with mean roughness below R_a = 5 nm on the sidewalls. The gratings were also optically characterised, showing good agreement with simulated results. The fabrication method demonstrated in this contribution shows the way for manufacturing high-quality diamond diffractive components that surpass existing devices both in quality and manufacturability.

1. Introduction

Diffraction gratings fabricated in single crystal diamond represent an inspiring endeavour, thanks to their exceptional material properties. Diamond exhibits a high refractive index (2.4 at 635 nm [1]) and low absorption over a wide spectral range spanning from ultraviolet to far infrared. Furthermore, it provides high thermal conductivity and a remarkably high laser induced damaged threshold (LIDT) [2]. These properties enable compact, high power laser components and spectrometers operating in the visible and UV range that are not accessible with other materials.

Diffraction gratings are key elements in the optical toolbox. A periodic change in the optical path length gives rise to interference, which can be exploited as a frequency selective element. Diffraction gratings are found in numerous optical systems, including monochromators [3], spectrometers [4–6], beamsplitters [7], continuous wave [8] and pulsed lasers [9]. These are commonly fabricated by mechanical ruling [10], where the grooves are created by mechanical material removal, or by microfabrication technologies based on photolithography and subsequent etching procedures [11]. While microfabrication is typically more complex, gratings fabricated this way are well suited as moulds for creating replicas [12].

Microfabrication also provides greater flexibility in patterning via lithography, gives access to a wide range of materials in addition to the typically employed grating substrates (quartz, plastic), such as silicon [13], gallium nitride [14] or gallium arsenide [15], and inherently enables surface treatments, such as distributed Bragg reflector (DBR) or anti-reflection (AR) coatings, in the same manufacturing environment. Current research efforts address the improvement of microfabricated gratings for astronomy [13], long-wavelength operation [16], microspectrometers [5,6] external cavity lasers [8] and large-area gratings [17,18]. In such applications, the extraordinary optical, mechanical and thermal properties of single crystal diamond are of high practical and functional value. Yet only recently has diamond been made commercially available as a single crystal substrate, thanks to the tremendous progress in

#373757 https://doi.org/10.1364/OE.27.030371
Journal © 2019 Received 26 Jul 2019; revised 4 Sep 2019; accepted 13 Sep 2019; published 7 Oct 2019

Optics EXPRESS

chemical vapour phase growth of high-quality plates [19–21]. Chemical inertness and mechanical hardness are the striking properties of diamond [22,23]. However, these properties cause significant challenges for microfabrication. As no chemical wet etchants exist for diamond, alternative microstructuring approaches, such as metal etching [24], laser ablation and modification [25–27], focused ion-beam milling [28], multi-photon UV etching [29,30] and dry etching [31] have been developed. The recent discovery of crystallographic diamond etching via unbiased oxygen plasma [32–34] allows the fabrication of microstructures revealing crystal planes selectively, in analogy to silicon processing via anisotropic etching with KOH/TMAH [35].

In this work, we demonstrate single crystal diamond diffraction gratings fabricated by photolithography, hardmask patterning and crystallographic etching. This method allows the definition of precise angles according to the crystalline planes of the substrate. We present diffraction gratings with sidewalls along the {100} and {111} planes, following our previous demonstration of this fabrication method to manufacture beamsplitters with trapezoidal profile [34]. Diffraction gratings in diamond have been previously published using directional anisotropic etching, exploitation of mask redeposition [36], boron implantation [37] and for X-ray applications [38]. Compared to these fabrication methods, crystallographic etching allows precise control of angles, produces smooth sidewalls free of ion damage and enables high aspect ratio gratings using commonly available microfabrication equipment. Furthermore, the here reported fabrication method facilitate the fabrication of blazed diffraction gratings, previously unobtainable in the diamond material system.

In this work we show the fabrication and detailed geometrical and optical characterisation of high-quality and uniform, large area gratings which are limited in quality only by substrate polishing and size. Furthermore, we elucidate the etch mechanism with numerical simulations.

2. Results

The diamond diffraction gratings were fabricated from commercially available general grade single crystal diamond substrates (Element Six, LakeDiamond). The grooves were lithographically defined and aligned to the <110> or <100> directions, determined optically from the substrate edge. A 60 nm thick Al_2O_3 hardmask protects the diamond during the unbiased oxygen plasma etching process (see Methods). Subsequent to the diamond crystallographic etching, the resulting gratings were characterised by scanning electron microscopy (SEM) and atomic force microscopy (AFM) to extract the geometry and surface roughness. The roughness on the top of the grooves only depends on the substrate polishing quality, as this area is not exposed to etching during processing.

The realised grooves in the <110> direction have a pitch and depth of 5 µm and 2.65 µm, respectively (Fig. 1(a)). We observed an asymmetry of the etched groove shape, which can be attributed to the misalignment of the gratings with respect to the <110> direction, resulting in an undercut of the mask (Fig. 1(b), dashed line). This effect is commonly observed in silicon gratings fabricated by crystallographic wet etching [39]. The angle of the gratings with respect to the surface plane is 57° (Fig. 1(b)). The sidewalls of the <110> groove are smooth with exception of steps occurring due to groove misalignment, yielding a total R_a of 22 nm. Exclusion of the steps results in a mean roughness (R_a) better than 5 nm (Fig. 2(a)).

The grooves in accomplished the <100> direction have a pitch and a depth of 4 µm and 1.37 µm, respectively (Fig. 1(c)). The AFM measurements revealed an almost vertical sidewall with an angle of 87° (Fig. 1(d)). We observed the sidewalls of the <100> grooves to be extremely smooth, with a measured R_a below 5 nm (Fig. 2(b)). We also noted the roughening on the bottom of the trenches, which we attribute to hardmask material remaining at the bottom of the trenches due to insufficient etching [40].

The efficiency of the diffraction orders in transmission was measured using a goniometer setup (see Methods), and the efficiency values were compared with simulated results based on

Optics EXPRESS

the extracted geometrical parameters (Fig. 3). The results show good agreement, indicating that the fabricated geometry approximates well ideal groove shape and spacing. We attribute the discrepancies between the measured and simulated values to fabrication non-uniformities due to grating pitch variation and roughness at the bottom of the <100> gratings. Additionally, we interferometrically measured wavefront uniformity of the fabricated gratings and found that the fabrication did not introduce significant variation to the optical path length. We report a RMS optical flatness of the diffraction grating $< \lambda / 3$ (peak-to-valley flatness: $< \lambda / 2$).

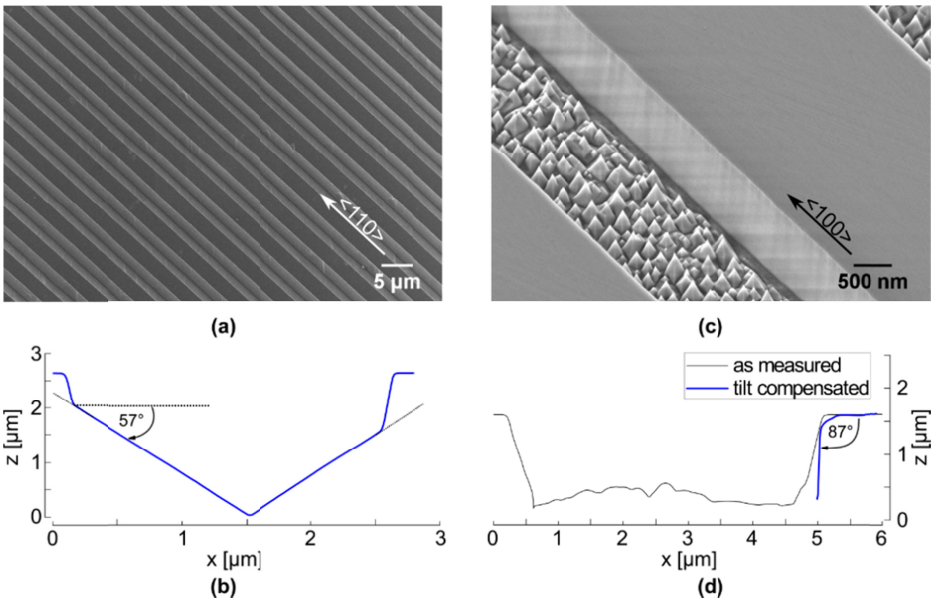

Fig. 1. **(a)** Scanning electron microscope (SEM) recording of <110> gratings revealing V-shaped grooves **(b)** extracted profile across a single V-groove in the <10> direction, showing hardmask undercut (true groove shape indicated with dashed line) and a 57° sidewall angle **(c)** SEM recording of <100> gratings showing a single grating groove with well-defined vertical sidewalls and **(d)** extracted profile across a single groove in <010> direction. The blue line corresponds to an AFM profile measured with a tilted sample and correction applied (see Methods).

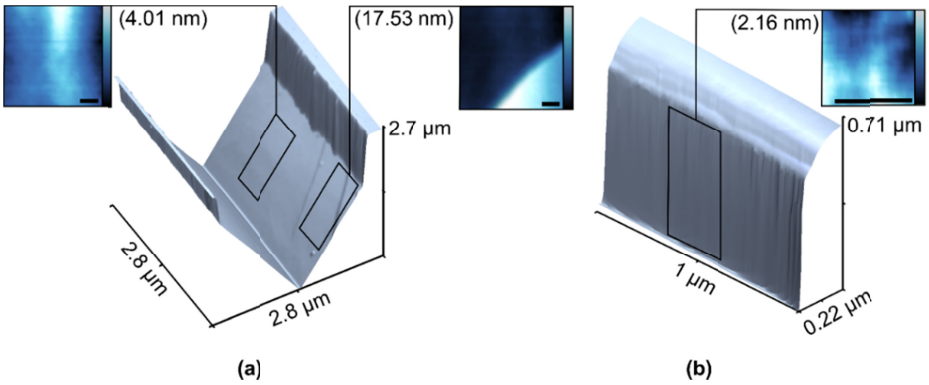

Fig. 2. Atomic force microscope (AFM) surface profile of a (a) <110> grating V groove and a **(b)** <100> grating vertical groove. Insets on panel **(a)** show the otherwise smooth sidewall featuring steps due to misalignment of the patterns to the true <110> direction, raising the overall roughness of the profile. In contrast, the sidewall of the vertical grooves show no steps and are uniformly smooth. Scale bars in insets are all 100 nm, mean roughness (Ra) is indicated in parentheses.

Optics EXPRESS

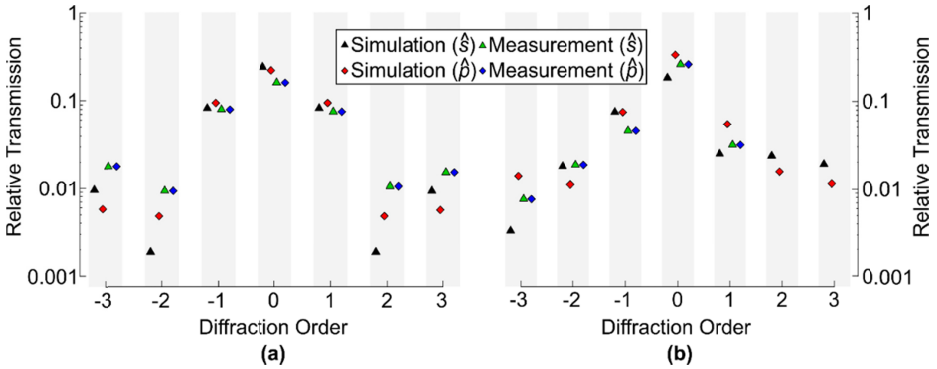

Fig. 3. Measured relative transmitted diffraction order efficiency for **(a)** <110> gratings, with a normal incidence beam, and **(b)** <100> gratings, with an oblique incident beam (φi = 41°), compared to simulated efficiencies. Both ŝ and p̂ polarisations are measured and calculated.

3. Discussion

Using a crystallographic etching procedure, we fabricated large area (4 mm^2), uniform gratings in single crystal diamond with precise angles. The groove shape depends on the pattern direction with respect to the crystal orientation. Both angled and vertical grating sidewalls have been experimentally demonstrated. The ability to fabricate vertical sidewall gratings indicates that the etch rate of the (100) plane is slower than that of the (110) plane. While the grating grooves aligned to the <100> crystal direction are close to vertical, we observed a deviation of the predicted groove angle of 54.7° between the (100) and (111) crystalline planes in the case of the grooves aligned to the <110> crystal direction. To explain the origin of this discrepancy, we modelled the crystallographic diamond etching based on previously developed models for crystallographic etching of single crystal silicon (continuous cellular automata method [41,42], see Methods). In agreement with the etch model, we attribute the angle difference to a directional anisotropic etching component. The directionality arises from an inherent biasing of the ICP plasma during diamond etching. We expect that this directionality can be tuned or even eliminated with the proper configuration of the plasma etcher, resulting in tuneable groove angles.

The etching process involves high density plasma to decrease the etching time. High power density heats up the substrate which leads to an isotropic surface roughening due to thermal etching [43]. Consequently, care must be taken to ensure good thermal contact with the backside cooled wafer. Extended etching times can lead to the deterioration of the thermal contact provided by the mounting wax. Thus, lowering the plasma density (by lowering ICP power) or cycling cooling steps [44] could be considered to decrease the thermal load.

Imprecise alignment causes undercut of the mask and shifting of the groove centreline, leading to groove asymmetry. This phenomenon is especially pronounced for long grooves and precise alignment of the groove direction with respect to the substrate is required for good control of the groove shape. An alignment technique used for silicon crystallographic etching is a pre-etch [45], where a first etch reveals a crystallographic plane to be used for subsequent alignment. This technique can be used to the same effect for diamond substrates. Another method is to utilise closed groove patterns, which limits the undercut due to trapping of atomic steps [39]. Further improvements in grating yield and groove surface quality can be achieved using higher grade surface polishing [46].

In conclusion, we have successfully manufactured diffraction gratings in a single crystal diamond with well-defined sidewall angles and smooth sidewalls, using a fabrication process based on hardmask deposition, lithography and oxygen plasma etching. Using a crystallographic dry etch, we fabricated grooves along <110> and <100> crystal directions, resulting in V-shaped and vertical groove profiles, respectively. We performed extensive geometrical

Optics EXPRESS

and optical characterisations to assess the quality of the produced devices. We have shown that the <110> grooves exhibit a sidewall angle of 57°, with a mean sidewall surface roughness of R_a = 22 nm, while the <100> grooves exhibit a sidewall angle of 87° and a roughness better than R_a = 5 nm. We have shown that the resulting devices are optically flat (peak-to-valley flatness:) and have diffraction efficiencies as predicted by simulations of the idealised groove profile, indicating uniform groove size and spacing and low scattering. Furthermore, it follows that such simulations are a reliable way of designing gratings based on this fabrication method.

To our knowledge, this is the first time diamond diffraction gratings fabricated via crystallographic etching are characterised in detail, showing that gratings fabricated with this method exhibit outstanding quality similar to the silicon system. We believe that this synergy allows the adaptation of existing designs for silicon-based diffractive elements to single crystal diamond, exploiting the broadband transmission window (including visible wavelengths) and the inherent high damage threshold. The shown fabrication method can be further refined to provide a scalable process enabling high-quality single crystal diffraction gratings, with smoother sidewalls and improved grating uniformity. While the grating pitch was chosen to showcase fabrication, the grating line resolution is a product of the lithography step and can be increased depending on the method used (the process shown can also be straightforwardly adapted to electron beam lithography if very fine pitch is required). Similarly, etch depth can be set by timing the etch process (vertical grooves) or by choice of pitch and duty cycle (V-shaped grooves).

The fabrication process can be adapted for the fabrication of blazed gratings (by exploitation of substrate miscut angle introduced groove angle asymmetry [47]), and the resulting low roughness surfaces are of great interest to manufacture low loss waveguide structures in diamond photonic integrated circuits.

4. Materials and methods

4.1. Microfabrication process

The microfabrication process is carried out on commercially available general grade single crystal diamond plates (Element Six, Lake Diamond) with dimensions of 2.6mm x 2.6mm x 0.3mm and <100> crystal orientation (Fig. 4). The plates are first cleaned in acetone and IPA, then 60 nm of Al_2O_3 is deposited using atomic layer deposition (ALD). Alumina represents an excellent hardmask for this etch process, with selectivity better than 1:80. The diamond plate is fixed to a wafer using mounting wax (QuickStick 135) to ensure thermal contact during diamond etching and facilitate handling. Subsequently photoresist (AZ ECI 3007) is spincoated onto the chip. The grating lines are exposed using contact lithography, aligned to the chip edges. Two samples were fabricated one with grating lines in the <110>, the other with grating lines in the <100> direction. The alumina hardmask is etched in a deep reactive ion etcher using chlorine chemistry (STS Multiplex). Afterwards, diamond etching is carried out using reactive ion etching (SPTS APS) with oxygen plasma, utilising high ICP power (2000 W) and zero platen bias power (15 mT process pressure, 30 sccm O_2 gas flow, 25 °C). Etching time was 70 minutes for the <110> gratings and 35 minutes for the <100> gratings, resulting in etch depths of 2.65 µm and 1.37 µm, respectively. After etching, the chip is released from the carrier wafer and the hardmask is stripped in concentrated hydrofluoric acid.

Optics EXPRESS

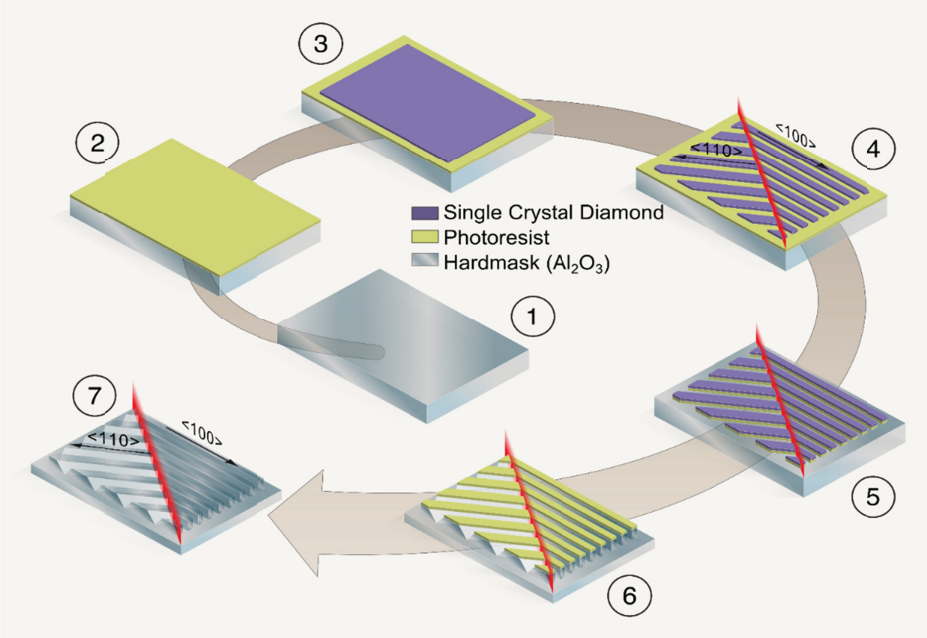

Fig. 4. Schematic representation of the microfabrication process for diffraction gratings in single crystal diamond: **1)** substrate cleaning **2)** Al_2O_3 deposition **3)** photoresist spincoating **4)** photoresist patterned with lines along either <110> or <100> direction **5)** alumina hardmask dry etch **6)** diamond dry etch resulting in grooves with profile dependent on direction.

4.2. Geometry characterisation

AFM was carried out on a Bruker FastScan using an EBD2-100A ultra-high aspect ratio probe (nanotools GmBH) (tip length: 2 µm). High aspect ratio tips are required for the measurements in order to accurately profile the roughness on the sidewalls and to measure the sidewall angle with respect to the surface, since using standard AFM tip geometries the sidewall surfaces cannot be reached. For the vertical sidewalls, the sample was tilted with respect to the probe cantilever (tilt angle 16°) to acquire accurate geometry and roughness. During post-processing the measured geometry was rotated by the tilt angle. In all cases, the scan direction was chosen to be perpendicular to the grooves and the probe symmetry axis to minimise the influence of the probe geometry. Reference angle measurements were taken on a KOH etched silicon sample to calibrate the measurements. Roughness values were taken from a groove sidewall with background removed to flatten the measured area. Angle measurements were also performed by SEM image analysis, and Focused Ion Beam (FIB) cross section, but were found to be limited in precision to 5°. Table 1 summarizes the measurement results.

Table 1. Summary of Measurements Results Using Ultra-High Aspect Ratio Tip Atomic Force Microscopy.

V-Groove angle	57.4° ± 3.3°
V-Groove surface roughness (R_a)	22 nm
Rectangular groove angle	87.47° ± 0.5°
Rectangular groove surface roughness (R_a)	5 nm

4.3. Optical measurement design and treatment

An optical measurement setup was built to measure the diffraction efficiency of the fabricated gratings (Fig. 5(a)). A low-power collimated diode laser (635 nm, 1.2 mW, Thorlabs) illumi-

Optics EXPRESS

nates the flat side of the grating mounted on a rotating stage. The diffraction orders are measured with a power sensor mounted on a goniometer. The distance of the power sensor to the sample (10 cm) was chosen to measure only a single order and to ensure the capture of the whole diffracted beam. The detector is rotated to measure the first 6 orders, and the peak values are recorded for each order. Oblique incidence is chosen for the <100> gratings to improve the contrast for the diffraction orders. At oblique incidence, orders higher than + 1 were clipped due to the sample mount and excluded from the results.

4.4. Interferometry

A Mach-Zehnder interferometric microscope [48] (Fig. 5(b)) was used in transmission to evaluate the optical flatness of the resulting diamond gratings. A 10X objective was used to take multiple phase images of the grating, subsequently stitched by digital image processing. The phase images of the gratings were numerically removed using a low pass Gaussian filter in MATLAB (with a radius of 60 μm^{-1}), then peak-to-valley and RMS optical path error was calculated.

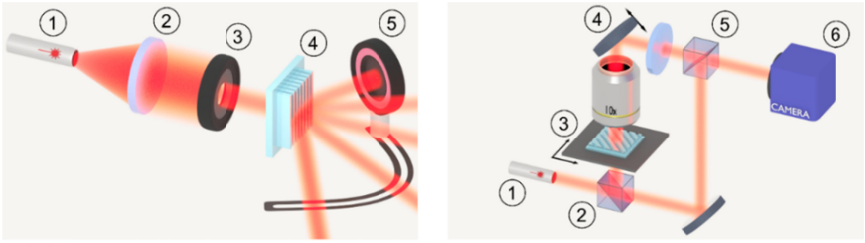

Fig. 5. **(a)** Schematic representation of the optical measurement setup to determine the grating diffraction efficiency. A 635 nm laser **(1)** is collimated **(2)** and sent through an iris **(3)** to match the grating **(4)** dimensions. A photodetector **(5)** is mounted on a goniometer and rotated around the sample. **(b)** Schematic representation of the Mach-Zehnder interferometric microscope for determination of the optical flatness of the diamond gratings. Light from a helium-neon laser **(1)** is split into equal beams **(2)**. One beam is incident on the sample mounted on a stage **(3)** and is collected by a 10x objective before encountering a variable phase shift produced by a piezo-mounted mirror **(4)**. The beams are recombined **(5)**, creating the interference image on the detector **(6)**.

4.5. Etch modelling

Modelling of the etch process for the grooves in the <110>/<100> direction was based on the continuous cellular automata method [41,42]. To account for the directional etching characteristic of reactive ion etching, the model was extended by including an additional etching component, applied only on cells in line-of-sight of the mask opening (e.g. directly exposed to the plasma). Only the planes of the lowest order ((100), (110), (111)) were modelled, under the simplification that influence of higher order planes can be neglected [41]. 2D profiles were extracted across trenches (in the <110> direction). Etch rates were fitted to the experimentally obtained profiles. Etch ratios of 0:1:20:10:10:25 ((100), (110), (111), directional-(100), directional-(110), directional-(111)) yield angles of 57.3° and 87.9°, respectively, simulated by our MATLAB Code 1 [49].

4.6. Diffraction grating modelling

The diffraction efficiency of the fabricated gratings were calculated with the RETICOLO package [50] using Rigorous Coupled Wave Analysis. The <110> gratings were approximated by a staircase function of 50 steps (53 nm step height) and both were calculated using 50 Fourier terms. The geometrical parameters were taken from the SEM and AFM measurements. Both $\hat{\mathbf{s}}$ and $\hat{\mathbf{p}}$ polarisations were extracted to compare against the measured values.

Optics EXPRESS

Funding

Swiss National Science Foundation (157566); Gebert Rüf Stiftung (GRS-043/16); European Research Council (ERC) (ERC-2015-AdG-695206 Nanofactory).

Acknowledgments

All microfabrication steps were performed at the Center for Micro- and Nanofabrication CMi at EPFL. The authors gratefully acknowledge the technical support of the CMi management and staff. The work has been supported by in-kind contribution of single crystal diamond substrates from LakeDiamond SA, a Swiss commercial supplier of cut and polished high purity single crystal diamond substrates.

References

1. F. Peter, "Uber brechungsindizes und absorptionskonstanten des diamanten zwischen 644 und 226 mu," Z. Phys. **15**(1), 358–368 (1923).
2. S. Reilly, V. Savitski, H. Liu, S. Reid, D. Gibson, H. Dhillon, S. O. Robbie, E. Gu, M. Dawson, A. Bennett, and A. Kemp, "Laser induced damage threshold of CVD-grown single crystal diamond surfaces with various surface finishes," in *Advanced Solid State Lasers, OSA Technical Digest (online)* (Optical Society of America, 2015), paper ATu2A.6.
3. L. Poletto, P. Miotti, F. Frassetto, C. Spezzani, C. Grazioli, M. Coreno, B. Ressel, D. Gauthier, R. Ivanov, A. Ciavardini, M. de Simone, S. Stagira, and G. De Ninno, "Double-configuration grating monochromator for extreme-ultraviolet ultrafast pulses," Appl. Opt. **53**(26), 5879–5888 (2014).
4. R. E. Bell, "Exploiting a transmission grating spectrometer," Rev. Sci. Instrum. **75**(10), 4158–4161 (2004).
5. Q. Nie, Z. Wen, and J. Huang, "A high-performance scanning grating based on tilted (111) silicon wafer for near infrared micro spectrometer application," Microsyst. Technol. **21**(8), 1749–1755 (2015).
6. J. Reimers, A. Bauer, K. P. Thompson, and J. P. Rolland, "Freeform spectrometer enabling increased compactness," Light Sci. Appl. **6**(7), e17026 (2017).
7. J. A. Davis and G. H. Evans, "Polarizing binary diffraction grating beam splitter," Opt. Lett. **29**(13), 1443–1445 (2004).
8. B. Mroziewicz, E. Kowalczyk, L. Dobrzanski, J. Ratajczak, and S. J. Lewandowski, "External cavity diode lasers with E-beam written silicon diffraction gratings," Opt. Quantum Electron. **39**(7), 585–595 (2007).
9. D. H. Martz, H. T. Nguyen, D. Patel, J. A. Britten, D. Alessi, E. Krous, Y. Wang, M. A. Larotonda, J. George, B. Knollenberg, B. M. Luther, J. J. Rocca, and C. S. Menoni, "Large area high efficiency broad bandwidth 800 nm dielectric gratings for high energy laser pulse compression," Opt. Express **17**(26), 23809–23816 (2009).
10. G. R. Harrison, "The production of diffraction gratings I. Development of the ruling art," J. Opt. Soc. Am. **39**(6), 413 (1949).
11. A. Labeyrie and J. Flamand, "Spectrographic performance of holographically made diffraction gratings," Opt. Commun. **1**(1), 5–8 (1969).
12. I. Yamada, Y. Ikeda, and T. Higuchi, "Fabrication of tunable diffraction grating by imprint lithography with photoresist mold," Rev. Sci. Instrum. **89**(5), 053110 (2018).
13. J. Ge, B. Zhao, S. Powell, A. Fletcher, X. Wan, L. Chang, H. Jakeman, D. Koukis, D. B. Tanner, D. Ebbets, J. Weinberg, S. Lipscy, R. Nyquist, and J. Bally, "Silicon immersion gratings and their spectroscopic applications," Proc. SPIE **8450**, 84502U (2012).
14. J. Lee, S. Ahn, H. Chang, J. Kim, Y. Park, and H. Jeon, "Polarization-dependent GaN surface grating reflector for short wavelength applications," Opt. Express **17**(25), 22535–22542 (2009).
15. G. Almuneau, M. Condé, O. Gauthier-Lafaye, V. Bardinal, and C. Fontaine, "High reflectivity monolithic sub-wavelength diffraction grating with GaAs/AlO $_x$ stack," J. Opt. **13**(1), 015505 (2011).
16. D. J. Mar, J. P. Marsh, C. P. Deen, H. Ling, H. Choo, and D. T. Jaffe, "Micromachined silicon grisms for infrared optics," Appl. Opt. **48**(6), 1016–1029 (2009).
17. W. G. Lu, R. Xiao, J. Liu, L. Wang, H. Zhong, and Y. Wang, "Large-area rainbow holographic diffraction gratings on a curved surface using transferred photopolymer films," Opt. Lett. **43**(4), 675–678 (2018).
18. J. Chen, H. Huang, Y. Zhang, Y. Wang, F. Kong, Y. Wang, Y. Jin, P. Chen, J. Xu, and J. Shao, "Reducing electric-field-enhancement in metal-dielectric grating by designing grating with asymmetric ridge," Sci. Rep. **8**(1), 5228 (2018).
19. I. Friel, "Optical quality diamond grown by chemical vapor deposition," in *Optical Engineering of Diamond* (John Wiley & Sons, Ltd, 2013), pp. 35–69.
20. A. Tallaire, V. Mille, O. Brinza, T. N. Tran Thi, J. M. Brom, Y. Loguinov, A. Katrusha, A. Koliadin, and J. Achard, "Thick CVD diamond films grown on high-quality type IIa HPHT diamond substrates from New Diamond Technology," Diamond Related Materials **77**, 146–152 (2017).
21. R. J. Nemanich, J. A. Carlisle, A. Hirata, and K. Haenen, "CVD diamond—Research, applications, and challenges," MRS Bull. **39**(6), 490–494 (2014).

Optics EXPRESS

22. S. J. Bull and A. Matthews, "Diamond for wear and corrosion applications," Diamond Related Materials **1**(10–11), 1049–1064 (1992).
23. J. E. Field, "The mechanical and strength properties of diamond," Rep. Prog. Phys. **75**(12), 126505 (2012).
24. M. Nagai, K. Nakanishi, H. Takahashi, H. Kato, T. Makino, S. Yamasaki, T. Matsumoto, T. Inokuma, and N. Tokuda, "Anisotropic diamond etching through thermochemical reaction between Ni and diamond in high-temperature water vapour," Sci. Rep. **8**(1), 6687 (2018).
25. C. L. Chao, W. C. Chou, K. J. Ma, T. T. Chen, Y. M. Liu, S. W. Huang, and H. Y. Lin, "Machining of CVD diamond film by RIE, laser ablation and thermo-chemical polishing(ultra-precision machining)," in *Proceedings of International Conference on Leading Edge Manufacturing in 21st century : LEM21* (2005), pp. 1063–1068.
26. V. I. Konov, "Laser in micro and nanoprocessing of diamond materials," Laser Photonics Rev. **6**(6), 739–766 (2012).
27. M. Martínez-Calderon, J. J. Azkona, N. Casquero, A. Rodríguez, M. Domke, M. Gómez-Aranzadi, S. M. Olaizola, and E. Granados, "Tailoring diamond's optical properties via direct femtosecond laser nanostructuring," Sci. Rep. **8**(1), 14262 (2018).
28. T. Graziosi, S. Mi, M. Kiss, and N. Quack, "Single crystal diamond micro-disk resonators by focused ion beam milling," APL Photonics **3**(12), 126101 (2018).
29. V. V. Kononenko, M. S. Komlenok, S. M. Pimenov, and V. I. Konov, "Photoinduced laser etching of a diamond surface," Quantum Electron. **37**(11), 1043–1046 (2007).
30. A. Lehmann, C. Bradac, and R. P. Mildren, "Two-photon polarization-selective etching of emergent nanostructures on diamond surfaces," Nat. Commun. **5**(1), 3341 (2014).
31. C. L. Lee, E. Gu, M. D. Dawson, I. Friel, and G. A. Scarsbrook, "Etching and micro-optics fabrication in diamond using chlorine-based inductively-coupled plasma," Diamond Related Materials **17**(7–10), 1292–1296 (2008).
32. B. Khanaliloo, M. Mitchell, A. C. Hryciw, and P. E. Barclay, "High-*Q*/*V* Monolithic Diamond Microdisks Fabricated with Quasi-isotropic Etching," Nano Lett. **15**(8), 5131–5136 (2015).
33. L. Xie, T. X. Zhou, R. J. Stöhr, and A. Yacoby, "Crystallographic orientation dependent reactive ion etching in single crystal diamond," Adv. Mater. **30**(11), 1705501 (2018).
34. M. Kiss, T. Graziosi, and N. Quack, "Trapezoidal diffraction grating beam splitters in single crystal diamond," Proc. SPIE **10513**, 105131K (2018).
35. D. B. Lee, "Anisotropic etching of silicon," J. Appl. Phys. **40**(11), 4569–4574 (1969).
36. P. Forsberg and M. Karlsson, "High aspect ratio optical gratings in diamond," Diamond Related Materials **34**, 19–24 (2013).
37. A. L. Stepanov, V. I. Nuzhdin, M. F. Galyautdinov, N. V. Kurbatova, V. F. Valeev, V. V. Vorobev, and Yu. N. Osin, "A diffraction grating created in diamond substrate by boron ion implantation," Tech. Phys. Lett. **43**(1), 104–106 (2017).
38. M. Makita, P. Karvinen, V. A. Guzenko, N. Kujala, P. Vagovic, and C. David, "Fabrication of diamond diffraction gratings for experiments with intense hard x-rays," Microelectron. Eng. **176**, 75–78 (2017).
39. S. Tan, R. Boudreau, and M. L. Reed, "Effects of mask misalignment and wafer misorientation on silicon v-groove etching," Sens. Mater. **15**(2), 101–112 (2003).
40. M. Challier, S. Sonusen, A. Barfuss, D. Rohner, D. Riedel, J. Koelbl, M. Ganzhorn, P. Appel, P. Maletinsky, and E. Neu, "Advanced fabrication of single-crystal diamond membranes for quantum technologies," Micromachines (Basel) **9**(4), 148 (2018).
41. O. Than and S. Büttgenbach, "Simulation of anisotropic chemical etching of crystalline silicon using a cellular automata model," Sens. Actuators Phys. **45**(1), 85–89 (1994).
42. Z. Zhu and C. Liu, "Micromachining process simulation using a continuous cellular automata method," J. Microelectromech. Syst. **9**(2), 252–261 (2000).
43. D. I. Shahin, T. J. Anderson, T. I. Feygelson, B. B. Pate, V. D. Wheeler, J. D. Greenlee, J. K. Hite, M. J. Tadjer, A. Christou, and K. D. Hobart, "Thermal etching of nanocrystalline diamond films," Diamond Related Materials **59**, 116–121 (2015).
44. P. Appel, E. Neu, M. Ganzhorn, A. Barfuss, M. Batzer, M. Gratz, A. Tschöpe, and P. Maletinsky, "Fabrication of all diamond scanning probes for nanoscale magnetometry," Rev. Sci. Instrum. **87**(6), 063703 (2016).
45. S. S. Singh, P. Pal, A. K. Pandey, Y. Xing, and K. Sato, "Determination of precise crystallographic directions for mask alignment in wet bulk micromachining for MEMS," Micro Nano Syst. Lett. **4**(1), 5 (2016).
46. S. Mi, A. Toros, T. Graziosi, and N. Quack, "Non-contact polishing of single crystal diamond by ion beam etching," Diamond Related Materials **92**, 248–252 (2019).
47. D. L. Voronov, E. M. Gullikson, and H. A. Padmore, "Ultra-low blaze angle gratings for synchrotron and free electron laser applications," Opt. Express **26**(17), 22011–22018 (2018).
48. C. Rockstuhl, I. Marki, T. Scharf, M. Salt, H. Peter Herzig, and R. Dandliker, "High resolution interference microscopy: a tool for probing optical waves in the far-field on a nanometric length scale," Curr. Nanosci. **2**(4), 337–350 (2006).
49. M. Kiss, "Crystallographic etch simulation code," https://doi.org/10.6084/m9.figshare.9116189.
50. J. P. Hugonin and P. Lalanne, *Reticolo Software for Grating Analysis* (2005).